Chaouch A, Porcelli V, Cox D, Edvardson S, Scarcia P, DeGrassi A, Pierri CL, Cossins J, Laval SH, Griffin H, Muller JS, Evangelista T, Topf A, Abicht A, Huebner A, vonderHagen M, Bushby K, Straub V, Horvath R, Elpeleg O, Palace J, Senderek J, Beeson D, Palmieri L, Lochmuller H.

Mutations in the Mitochondrial Citrate Carrier SLC25A1 are Associated with Impaired Neuromuscular Transmission.

***Journal of Neuromuscular Diseases* 2014, 1(1), 75-90.**

Journal of Neuromuscular Diseases 1 (2014) 75–90
DOI 10.3233/JND-140021
IOS Press

Research Report

Mutations in the Mitochondrial Citrate Carrier SLC25A1 are Associated with Impaired Neuromuscular Transmission

Amina Chaouch[a], Vito Porcelli[b], Daniel Cox[a], Shimon Edvardson[c], Pasquale Scarcia[b], Anna De Grassi[b], Ciro L. Pierri[b], Judith Cossins[d], Steven H. Laval[a], Helen Griffin[a], Juliane S. Müller[a], Teresinha Evangelista[a], Ana Töpf[a], Angela Abicht[e,f], Angela Huebner[g], Maja von der Hagen[g], Kate Bushby[a], Volker Straub[a], Rita Horvath[a], Orly Elpeleg[c], Jacqueline Palace[h], Jan Senderek[f], David Beeson[d], Luigi Palmieri[b,i] and Hanns Lochmüller[a,*]

[a]*Institute of Genetic Medicine, MRC Centre for Neuromuscular Diseases, Newcastle University, Newcastle upon Tyne, UK*
[b]*Department of Biosciences, Biotechnology and Biopharmaceutics, University of Bari Aldo Moro, Bari, Italy*
[c]*Monique and Jacques Roboh Department of Genetic Research, Hadassah, Hebrew University Medical Center, Jerusalem, Israel*
[d]*Neurosciences Group, Nuffield Department of Clinical Neurosciences, University of Oxford, John Radcliffe Hospital, Headley Way, Oxford, UK*
[e]*Medizinisch Genetisches Zentrum, Munich, Germany*
[f]*Friedrich-Baur-Institut, Ludwig Maximilians University, Munich, Germany*
[g]*Children's Hospital, Technical University Dresden, Dresden, Germany*
[h]*Department of Clinical Neurology, The John Radcliffe, Oxford, UK*
[i]*CNR Institute of Biomembranes and Bioenergetics, Bari, Italy*

Abstract.
Background and Objective: Congenital myasthenic syndromes are rare inherited disorders characterized by fatigable weakness caused by malfunction of the neuromuscular junction. We performed whole exome sequencing to unravel the genetic aetiology in an English sib pair with clinical features suggestive of congenital myasthenia.
Methods: We used homozygosity mapping and whole exome sequencing to identify the candidate gene variants. Mutant protein expression and function were assessed *in vitro* and a knockdown zebrafish model was generated to assess neuromuscular junction development.
Results: We identified a novel homozygous missense mutation in the *SLC25A1* gene, encoding the mitochondrial citrate carrier. Mutant SLC25A1 showed abnormal carrier function. *SLC25A1* has recently been linked to a severe, often lethal clinical phenotype. Our patients had a milder phenotype presenting primarily as a neuromuscular (NMJ) junction defect. Of note, a previously reported patient with different compound heterozygous missense mutations of *SLC25A1* has since been shown to suffer from a neuromuscular transmission defect. Using knockdown of SLC25A1 expression in zebrafish, we were able to mirror the human disease in terms of variable brain, eye and cardiac involvement. Importantly, we show clear abnormalities in the neuromuscular junction, regardless of the severity of the phenotype.
Conclusions: Based on the axonal outgrowth defects seen in SLC25A1 knockdown zebrafish, we hypothesize that the neuromuscular junction impairment may be related to pre-synaptic nerve terminal abnormalities. Our findings highlight the complex machinery required to ensure efficient neuromuscular function, beyond the proteomes exclusive to the neuromuscular synapse.

Keywords: Congenital myasthenic syndrome, neuromuscular junction, mitochondrial citrate carrier, SLC25A1

*Correspondence to: Hanns Lochmüller, Institute of Genetic Medicine, International Centre for Life, Newcastle University, Newcastle upon Tyne, NE1 3BZ, UK. Tel.: +44 191 2418602; Fax: +44 191 2418770; E-mail: hanns.lochmuller@ncl.ac.uk.

ISSN 2214-3599/14/$27.50

INTRODUCTION

Congenital myasthenic syndromes (CMS) are a group of inherited neuromuscular disorders in which the integrity of the neuromuscular junction (NMJ) is compromised [1]. The clinical hallmark of these syndromes is fatigable weakness, which is often treatable. Most of CMS patients present with fluctuating ocular, bulbar, respiratory and limb weakness [2, 3]. Over the past 25 years, more than 19 genes have been implicated in congenital myasthenic syndromes [4, 5]. These usually express proteins involved in neuromuscular synapse development and function; and most mutations identified so far have involved post-synaptic proteins.

However, in spite of recent progress, a proportion of congenital myasthenic syndrome patients remain genetically undiagnosed [2]. Thus, one can speculate that some of these undiagnosed patients may harbour very rare private mutations in a particular gene. Alternatively, these patients may have mutations in genes encoding ubiquitous proteins that can primarily present as an NMJ defect but may also have a much broader spectrum of disease. A good example includes the recently discovered CMS related to mutations in genes that were until then implicated in congenital glycosylation disorders [6, 7]. Another example includes mutations in *PLEC1* and *LAMB2* genes in which mutations can lead to a CMS phenotype combined with skin or kidney disease respectively [8, 9].

Whilst mitochondrial gene defects can cause a myriad of neurological disorders including myopathies and neuropathies, these have not been specifically implicated in defects of the neuromuscular junction [10, 11].

SLC25A1 is a mitochondrial citrate carrier believed to be a key player in fatty acid and sterol biosynthesis, gluconeogenesis and glycolysis [12]. More recently, it has been proposed that it may also play a role in the maintenance of chromosome integrity and in the regulation of autophagy [13, 14].

In the mitochondria, SLC25A1 mediates the exchange of mitochondrial citrate/isocitrate with cytosolic malate. The exported citrate is cleaved into acetyl-coenzyme-A and oxaloacetate by ATP-citrate lyase [12, 15]. Acetyl-coenzyme A is the main substrate of lipid and sterol biosynthesis in the cell while oxaloacetate is usually reduced to malate and diverted back into the mitochondria for further exchange with mitochondrial citrate. Citrate can also inhibit cytosolic phosphofructokinase 1, thus indirectly influencing the rate of glycolysis. Both citrate and malate are involved in regulating NADPH content in the cell [15, 16].

The recent discovery of several patients harbouring mutations in this mitochondrial carrier has confirmed that this is a protein of critical biological importance in humans [17, 18]. Indeed SLC25A1 dysfunction was shown to interfere with brain, eye and perhaps neuromuscular development, in addition to causing a distinctive urinary organic acid profile. Whether this metabolic disturbance itself is sufficient to explain the phenotype is unclear at present. However, it is likely that other factors like oxidative stress, ROS toxicity and NADPH content are also relevant.

We performed whole exome sequencing in an affected sib pair from a consanguineous family from Northern England. The patients had remained genetically undiagnosed for more than 23 years, having had a suspected clinical diagnosis of congenital myasthenia with a reported response to pharmacotherapy.

MATERIALS AND METHODS

Patient data

Patients were selected from the Newcastle MRC Neuromuscular Centre, Institute of Genetic Medicine, Newcastle upon Tyne. Our patients were 2 Caucasian siblings born to two healthy consanguineous parents (first cousins), from Newcastle in the North of England. The index case was a male patient who presented with fatigable weakness since early infancy mainly involving his limbs. Neurophysiological studies showed no evidence of neuropathy or myopathy. Although there was no decrement on repetitive nerve stimulation, there was marked jitter in several muscles in keeping with impaired neuromuscular junction transmission. His sister presented in a similar fashion but exhibited moderate intellectual disability. Given the positive family history, evidence of fatigable weakness with abnormal jitter, a diagnosis of CMS was suspected. Appropriate consent for research was obtained from each patient and any family member involved in this study.

Genomic DNA was extracted from venous blood taken from both siblings and unaffected family members, by automated DNA extraction on the M48 Bio Robot using the MagAttract DNA blood Mini M48 kit (Qiagen 951336) as part of the routine service performed by the Northern Genetics Service molecular laboratory.

Study of the patient neuromuscular junction

Repetitive nerve stimulation and single fibre EMG (SFEMG) were carried out on the index case at age 20

and repeated at 21 years. 3 Hz stimulation was used to search for decrement and we checked for facilitation after 20 sec of voluntary maximum contraction.

The number of endplate AChR was determined as previously described [19]. Briefly, muscle bundles were dissected, labelled with 125I-a-BuTX, prior to staining for acetylcholinesterase. The number of endplates in a given region was determined in combination with respective level of 125I-a-BuTX binding to generate the number of receptors per endplate. 35 NMJ were checked to determine (miniature endplate potentials (MEPPS) and quantal content with between 1 and 62 MEPPS per NMJ.

Homozygosity mapping

In order to identify the chromosomal location of the disease causing mutation in this family, we carried out genome wide genotyping of SNPs using Illumina 300K chip (Illumina, San Diego, Ca). This was performed to identify regions of homozygosity shared by both affected siblings, since we presumed the inherited disease to be recessive caused by a homozygous mutation segregating on the same ancestral haplotype.

Whole exome sequencing and data analysis

Given that the family history was highly suggestive of autosomal recessive inheritance (healthy parents, two affected children and parental consanguinity), and that most CMS are recessive in inheritance, we applied the recessive model looking for genes containing homozygous or at least 2 heterozygous changes shared between siblings (see supplementary material for the details of exome filtering pipeline).

CGH array analysis

CGH array was carried out to analyse copy number variations on the female patient who exhibited intellectual disability. CytoChip ISCA 180 K V1.0 oligonucleotide array (BlueGnome) was used according to the manufacturer´s instructions (BlueGnome). *Rsa*I and *Alu*I digested DNA products (patient's DNA as well as reference DNA) from peripheral blood were labelled by random priming using either Cy3-dUTP or Cy5-dUTP) and hybridized at 65°C for 24 h. Scanning and image acquisition was done on an Agilent microarray scanner. Data analysis was performed using BlueFuse Multi software (BlueGnome).

Construction of the expression plasmids and bacterial expression

The coding sequence of the yeast orthologue citrate carrier CIC (CTP1, NM_001178639.1) was amplified from S. cerevisiae genomic DNA via PCR and the mutations were introduced by site-directed mutagenesis as described in QuikChange® Site-Directed Mutagenesis Kit from Stratagene. Ctp1p and its mutated form (p.R241Q, p.R276H and p.G117D) were overexpressed as inclusion bodies in the cytosol of E. coli strain BL21 (DE3). Inclusion bodies were purified on a sucrose density gradient and washed at 4°C, first with Tris-EDTA buffer (10 mM Tris–HCl, 1 mM EDTA, pH 7.0), then twice with a buffer containing Triton X-114 (3%, w/v), 1 mM EDTA, 20 mM Na_2SO_4 and 10 mM PIPES pH 7.0, and finally with the Tris-EDTA buffer pH 7.0. The proteins were solubilized in 1.7% sarkosyl (w/v). Eventual small residues were removed by centrifugation (20800 × *g* for 10 min at 4°C).

Reconstitution of the recombinant proteins into liposomes and transport assays

The recombinant proteins solubilized in sarkosyl were reconstituted by cyclic removal of detergent as described [20] with some modification. The reconstitution mixture consisted of phospholipids in the form of sonicated liposomes (10 mg), protein solution (25 µl, about 9 µg), 10% Triton X-114 (70 µl), 10 mM citrate (35 µl), cardiolipin (0.7 mg), 10 mM PIPES/NaOH pH 7.0 and water (final volume 700 µl). The mixture was recycled 13-fold through an Amberlite column pre-equilibrated with 10 mM PIPES-NaOH (pH 7.0) and 50 mM NaCl. All operations were performed at 4°C except the passages through Amberlite, which were carried out at room temperature. Approximately 20% of WT or mutated CIC proteins were reconstituted. External citrate was removed from proteoliposomes on Sephadex G-75 columns pre-equilibrated with 50 mM NaCl and 10 mM PIPES at pH 7.0 (buffer A). Transport at 25°C was started by adding 0.1 mM [^{14}C] Citrate (from PerkinElmer, Inc) to proteoliposomes and terminated by addition of 20 mM pyridoxal 5′ phosphate and 20 mM of bathophenanthroline. In controls, inhibitors were added with the labelled substrate. The external substrate was removed by Sephadex G-75 columns pre-equilibrated with buffer A, and the entrapped radioactivity was counted. The experimental values were corrected by substracting control values and the initial transport rate was calculated from the

time-course of substrate uptake by proteoliposomes [21].

Mitochondrial membrane potential assessment in fibroblasts

Fibroblasts from the affected sibling harbouring the *SLC25A1* variant c.740G > A; p.R247Q and control fibroblasts were grown in DMEM (high glucose). Membrane potential was measured by fluorescence microscopy using the tetramethylrhodamine methyl ester (TMRM) probe [22], while mitochondrial morphology was investigated using MitoTracker® Red CMXRos. MitoTracker® Red CMXRos and tetramethylrhodamine methyl ester (TMRM) were purchased from Life Technologies.

Fluorescent images of treated cells were acquired and fluorescence intensities were analyzed, as previously described [23], using a Zeiss Axiovert 200 microscope equipped with a Photometrics Cascade 512B CCD camera (Roper Scientific) and the MetaFluor software (Universal Imaging).

Western blotting

Immunoblot analysis was performed using 100×10^3 cells (patient and control fibroblast). The cells were rinsed with ice-cold PBS and lysed using RIPA buffer. Total proteins were heated at 100°C for 5 min, separated by SDS-PAGE and transferred to nitrocellulose membranes. The membrane was then incubated at room temperature with anti-SLC25A1 polyclonal antibodies raised in rabbit against recombinant rat SLC25A1 carrier or mouse monoclonal antibodies against the β subunit of human F1-ATPase (BD Biosciences). Antigen–antibody complexes were detected using anti-rabbit or mouse IgG-coupled horseradish peroxidase (Pierce, Thermo Scientific), in combination with the ECL system (Merk Millipore).

Multiple sequence alignment and evolutionary pressure analysis

A multiple sequence alignment of citrate carrier (CIC) orthologs from various species and other mitochondrial carriers was obtained using ClustalW [24]. The functional or structural relevance of the mutated residues of the mitochondrial citrate carrier protein was estimated according to a scoring system based on the evolutionary pressure acting on each amino acid as described previously [25].

SLC25A1 knockdown in zebrafish embryos

A BLAST search of zebrafish transcripts with the human SLC25A1 protein sequence as input revealed the presence of three homologues in the zebrafish genome: two on chromosome 10: SLC25A1a (NM_200607), SLC25A1b (XM_003199276.2) and one on chromosome 8 (SLC25A1c). Only SLC25A1a and SLC25A1b from chromosome 10 are expressed in zebrafish (Supplementary Figure 1).

Zebrafish husbandry and observation

The Golden strain (*slc24a5*$^{b1/+}$) of zebrafish was used in this study (Zebrafish International Resource Centre (ZIRC), Oregon). Zebrafish embryos were raised at 28.5°C and staged in hours or days post-fertilization (hpf or dpf) according to standard procedures. Video recordings of embryos and larvae were taken with a Leica dissection stereomicroscope equipped with a Chameleon digital camera (model CMLN-13S2M, Chameleon). Touch-evoked swimming response of embryos was elicited by touching the head or the tail of the embryos with a fine pipette tip. Light microscope images of injected and non-injected embryos were taken with a digital camera (model LEICA DFC 420C) mounted on a Leica dissection stereomicroscope. Procedures involving experimentation on animal subjects were done in accordance with the local institutional guide.

Antisense morpholino oligonucleotide knockdown

Antisense morpholino oligonucleotides (MOs) were purchased from Gene Tools LLC (Pilomath, OR). The MOs were designed with the mRNA sequence of the zebrafish *SLC251A* orthologues and genomic sequences available from public databases (SLC25A1A GeneID: 393579, accession number: NM_200607.1) and (SLC25A1B GeneID: 795332, accession number: XM_003199276.2) and the corresponding genomic DNA sequence obtained from the zebrafish chromosome 10 assembly.

We established two MOs, one per gene orthologue. Both MOs are splice-blocking and directed against the splice donor site of exon 3. The following two morpholinos were used: (MO1: zSLC25A1a 5′-AGATGAATCTTTCTTACCGTACTGC-3′ and MO2: zSLC25A1b 5′-GCGGGTTAGGAAACACTCACCTCAC-3′). Both MOs are expected to interfere with the splicing process and lead to a disruption of the protein open reading frame and premature

translation termination after 25 missense amino acids. The Gene Tools standard control MO (5′-CCTCTTACCTCAGTTACAATTTATA-3′) targeting a human beta-haemoglobin gene was used as a negative control for the effects of MO injection. We also used the Gene Tools anti-p53 MO (5′-GCGCCATTGCTTTGCAAGAATTG-3′) to suppress any non-specific apoptotic effects that can be induced by some MOs.

MOs were suspended in 1x Danieau solution (58 mM NaCl, 0.7 mM KCl, 0.4 mM MgSO4, 0.6 mM Ca(NO3)2, 5 mM HEPES; pH 7.6) with phenol red as an injection indicator.

Embryos were injected with both morpholinos separately to determine the optimal concentration to produce the best range of phenotypes and then with both MOs simultaneously. 5 ng SLC25A1a MO and 2.5 ng SLC25A1b produced the best range of phenotypes. Four independent MO injection experiments were performed for each MO and at least 500 injected embryos were evaluated in total for each MO.

RNA isolation and RT-PCR

RNA from approximately 30 zebrafish embryos was isolated with Trizol reagent (Invitrogen, Life Technologies) following the manufacturer's instructions. Reverse transcription was performed with 1 or 2 μg total RNA as template with the Superscript III First-Strand Synthesis System (Invitrogen, Life Technologies) and MolTaq DNA polymerase (Molzym). Regions of interest were amplified with compatible primers.

Immunofluorescence staining

Whole-mount immunofluorescence staining and imaging of zebrafish embryos was conducted as previously described. In brief, NMJ were visualized with Alexa Fluor® 594 conjugated alpha-bungarotoxin (Invitrogen, Life Technologies, 1 mg/ml) and a mouse monoclonal anti-SV2 (synaptic vesicle protein 2) antibody (Developmental Studies Hybridoma Bank, Iowa City, IA; dilution 1:200). Alexa Fluor® 594 conjugated phalloidin (Sigma-Aldrich) was used at a concentration of 5 μg/ml to label actin.

RESULTS

Clinical phenotype

This was a consanguineous family of Caucasian origin from the north of England with 2 affected siblings and one healthy offspring. Both parents were reportedly healthy. The index case is a 33-year-old man who was the product of normal pregnancy and birth but displayed some speech and motor developmental delay. In early childhood, he developed intermittent leg weakness, which was exercise induced and improved with rest. He had no ocular, bulbar or respiratory difficulties. He had mild learning difficulties but was able to attend mainstream schooling and settle in full time employment. His neuromuscular symptoms have been stable over the years. Of note, he recently developed obsessive-compulsive tendencies. Examination showed mild bilateral ptosis but no ophthalmoplegia. He has dysarthria with fatigable speech. Muscle tone and power were normal at rest. However, there was fatigability with exercise. He had bilateral pes cavus as well as calf hypertrophy bilaterally. Reflexes were reduced at rest with clear potentiation with exercise (Table 1).

The sister, who is now 19 years, is the product of normal pregnancy and birth. She had delayed psychomotor milestones, more marked than her brother. She developed recurrent falls in early infancy with clear fatigable weakness in all her limbs. She complained of intermittent double vision but she had no bulbar or respiratory difficulties. The course of her illness was static. Examination showed some facial weakness with no ophthalmoplegia or ptosis. She had mild neck flexion weakness with fatigable arm and leg weakness. She is ambulant. Reflexes were normal. This patient currently attends a special need college (Table 1).

Neurophysiology was performed in consecutive years when the index patient was aged 20 and 21 years with similar outcome. At both examinations, repetitive nerve stimulation of ADM (*abductor digiti minimi*) and *anconeus* at 3 Hz stimulation showed no decrement of CMAP (compound muscle action potential) and no facilitation of CMAP after maximum voluntary contraction for 20 sec. SFEMG (single fibre EMG) on EDC (*extensor digitorum communis*) showed 72% of potential pairs have increased jitter or jitter with blocking: −25% were normal, 52% showed increased jitter, 20% showed block, from 25 pairs sampled. Analysis of jitter showed a MCD (mean consecutive difference) of 78.5 ± 44.4 micros from non-blocking pairs. At age 21, SFEMG on EDC showed 81% of potential pairs have increased jitter or jitter with blocking: 19% were normal, 62% showed increased jitter, 19% were blocking, from 16 pairs. MCD was 71.6 micros.

Muscle biopsy was normal although electron microscopy of an earlier muscle biopsy suggested enlarged mitochondria and an increase in their number.

Table 1
Clinical features of the 3 patients with mutations in the *SLC25A1* gene presenting with a phenotype suggestive of congenital myasthenia

	Case 1	Case 2	Case 3
Gender/age/ethnicity	Male/33y/English	Female/19y/English	Female/18 m/Israeli
Mutation	p.R247Q	p.R247Q	p.G130D; p.R282H
Progression	Stable with some long term fluctuations	Stable	progressive
Age at onset	Less than 2 years	Less than 2 years	10 days
Symptoms at onset	Fluctuating leg weakness	Fluctuating arm and leg weakness	Poor suck, hypotonia, apneas
Psychomotor delay/intellectual disability	No but developed obsessive compulsive disorder in adulthood	Yes	Yes
Ocular involvement	Ptosis	Ptosis	Optic nerve hypoplasia
Bulbar weakness	No	No	Yes
Apneic crises	No	No	Yes
Epilepsy	No	No	Yes
Agenesis of the corpus callosum	No	No	Yes
Hearing loss	No	No	Yes
Elevated urinary organic acids	No	No	Yes
Abnormal jitter with block	Yes	Not done	Yes
Positive response to treatment	Yes	Equivocal	No

We were unable to access the biopsy to obtain further details. Only a crude determination of endplate morphology was obtained at the time. In some cases the endplates appeared enlarged, but there are not detailed studies of this. Analysis of an anconeus muscle biopsy showed normal endplate AChR number. Consistently MEPP amplitude and quantal content in *in vitro* electrophysiology was within the normal range.

Muscle histology was normal with normal respiratory chain enzyme activity and no evidence of mitochondrial DNA deletions on muscle analysis. Blood and CSF lactate levels were normal. Genetic testing for MELAS, MERRF, LHON, NARP was negative. Free and total carnitine levels were normal. Acetylcholine receptor antibodies were negative. CT and more recently MRI of the brain with spectroscopy were normal.

The index case was initially treated with pyridostigmine with no clear benefit after which he was instigated on 3,4-DAP with a favourable response. His sister received pyridostigmine since early childhood, which she continues to this date. It is unclear whether she has any benefit from this treatment.

While the index case had normal karyotype, we identified a 30.4 Mb deletion Xq25 to Xq28, Position 122,440,897-154,886,079 using CGH array in the affected sister. The parents have not yet been tested for this deletion.

The third patient was described earlier and is now aged 3 years [17]. She presented soon after birth with poor sucking, recurrent apnoea, apathy and hypotonia. Corpus callosum agenesis and optic atrophy were found. Subsequently, psychomotor developmental delay, reduced spontaneous movement as well as seizures were documented. Recurrent apnoea and poor respiratory effort necessitated tracheostomy. She is now ventilator-dependent. Urinary organic acid analysis revealed a large peak of 2-hydroxyglutaric acid and Krebs cycle intermediates. Mitochondrial functions in cultured skin fibroblasts disclosed decreased growth in glucose free medium, increased ROS production and decreased mitochondrial membrane potential but normal ATP content. Exome sequencing led to the identification of two *SLC25A1* variants, chr.22:19163734 C->T resulting in (p.R282H) and chr.22:19165292 C->T resulting in (p.G130D). Kinetic studies using mutant recombinant protein into liposomes showed complete loss of transport function for the former variant and only a small residual activity for the latter. Single-fibre EMG at the age of 2 years revealed markedly increased jitter and blocking. The myasthenic symptoms did not fluctuate and did not improve with 3,4-DAP, pyridostigmine and ephedrine (Table 1).

Our two affected siblings were born to healthy consanguineous parents indicating a recessive pattern of inheritance. The following CMS genes were excluded by targeted linkage analysis: *COLQ, CHRNA1, CHRNB1, CHRNE, CHAT, RAPSN, MUSK, SCN4A, DOK7* and *GFPT1*. Sanger sequencing was carried out to further exclude *CHRNA1, CHRNB1, CHRND, CHRNE, RAPSN, CHAT, DOK7* and *COLQ*.

Identification of mutations in SLC25A1 gene

Homozygosity mapping by genome wide SNP genotyping revealed 4 large homozygous blocks on chromosome 5 (7.97 Mb); chromosome 13 (19.43 Mb); chromosome 16 (17.02 Mb) and chromosome 22

(10.62 Mb) shared by both siblings. Because these homozygous blocks were very large and contained many genes, we decided to proceed with whole exome sequencing in both siblings.

Whole exome sequencing generated an average of 8.73 gigabases (Gb) of mappable sequences per patient and 53.92% of reads mapped to targets. 87% of targeted variants had a 10 fold coverage, which was used for variant calling in our filtering pipeline. Filtering of variants shared by both siblings by restricting our search to coding, rare (frequency <1%), predicted to be deleterious changes, allowed us to shortlist one homozygous variant in the *SLC25A1* gene (exon7: c.740G > A; p.R247Q, GenBank: NM_005984). This variant was located in the large homozygous block on chromosome 22 and led to the substitution of a highly conserved positively charged arginine residue to a neutral glutamine residue. It is worth noting that the same mutation was identified using whole genome sequencing of the older sibling. A second rare variant was identified in *CLTL1*, c.719A > G; p.N240S (rs147685377). However, this variant was identified

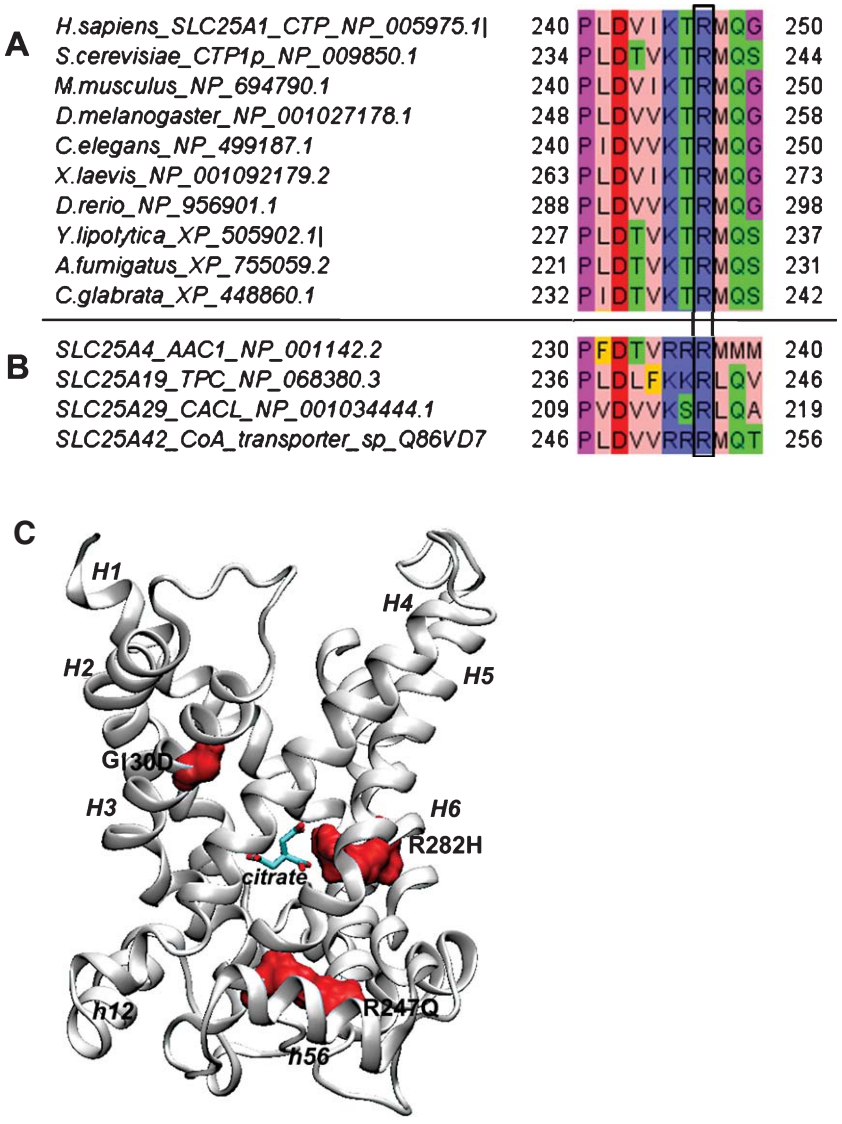

Fig. 1. Sequence alignment of mitochondrial citrate carrier (SLC25A1) from different organisms (panel A) and other members of mitochondrial carrier family (panel B). Accession numbers for each species/carrier is given. Panel C shows structural comparative model of human CIC and docking of citrate. The 3D comparative model of human CIC is reported in white cartoon representation. The six transmembrane helices are indicated by black labels (H1-H6). Two of the three helices parallel to the membrane planes are also labelled (h12 and h56). The citrate ligand is shown in cyan licorice. The pathogenic mutations p.R247Q (this work), p.G130D, p.R282H [17] are displayed in red surf representation.

at frequencies between 0.1% and 0.7% in public and "in house" databases suggesting that this is likely to be a benign variant.

The *SLC25A1* variant (c.740G > A; p.R247Q) segregated in the family according to an autosomal recessive transmission pattern. Both parents were heterozygous for the mutant allele whilst the unaffected brother was homozygous for the wild type allele.

We further screened a total of 58 patients from our CMS cohorts (Munich, Newcastle, Oxford), but did not identify additional pathogenic variants in *SLC25A1*. Exome sequencing of 100 undefined neuromuscular cases including CMS cases did not identify any other *SCL25A1* variants.

After obtaining the above described results, we proceeded to investigate a neuromuscular transmission defect in a Jewish Ashkenazi patient (patient 3 described above), previously described by us with compound heterozygous disease-causing mutations of *SLC25A1* gene [17].

Biochemical characterization of the SLC25A1 variants

SLC25A1 consists of eight exons which encode the mitochondrial citrate carrier, a 311 amino acid protein. The percentage of identical amino acids between the yeast and the mammalian orthologous mitochondrial carriers is generally not much higher than that observed between the different members of the mitochondrial carrier family (25–30% of identical amino acids; [26]). Notably the yeast Ctp1p shares 37% of sequence identity (52% of sequence similarity) with the human citrate transporter coded by SLC25A1. Nonetheless, S. cerevisae has been shown to be useful for studying the functional effect of pathogenic mutations in human mitochondrial transporters that proved difficult to be over-expressed in bacteria [17, 27]. As shown in Fig. 1A, arginine 247 is highly conserved in SLC25A1 of *fungi* and *metazoan* and also conserved in several other mitochondrial carriers (Fig. 1B). This residue belongs to the transmembrane helix 5 and corresponds to the second basic amino acid of the sequence motif PX[D/E]XX[K/R]X[K/R], which is characteristic of members of the mitochondrial carrier family [28]. By comparison with the crystallized structure of the ADP/ATP carrier [29] it is observed that R247, together with the two residues of the citrate carrier located at the same height on transmembrane helix 1 (Q52) and 3 (K149), is involved in ionic interactions with the acidic residues of the second part of the MCF sequence motif [D/E]Gx5Ar[K/R]G at the beginning of even transmembrane helices (Fig. 1c, Supplementary Figures 2, 3). These intra-repeat interactions participate in alternate closing and opening of the carrier on the matrix side during the substrate transport cycle [30].

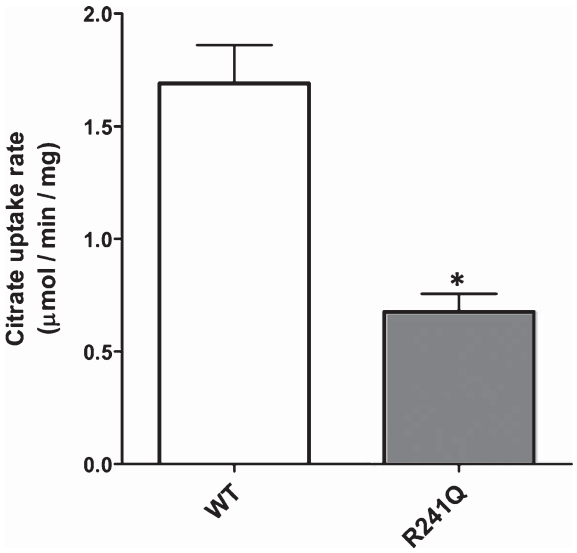

Fig. 2. Functional characterization of the wild-type (WT) and the p.R241Q Ctp1. The uptake rate of (^{14}C) citrate was measured by adding 0.1 mM of (^{14}C) citrate to proteoliposomes reconstituted with purified WT or with the mutated Ctp1 protein. The proteoliposomes were preloaded internally with 10 mM of citrate. The means and SDs from five independent experiments are shown (*$p < 0.01$, two-tailed unpaired Student's *t*-test).

Kinetic analysis of the R241Q Ctp1p mutant was performed upon reconstitution of purified recombinant protein into liposomes. As shown in Fig. 2, the substitution of R241, corresponding to R247 in human SLC25A1, with glutamine causes a strong impairment of transport activity compared to WT Ctp1p even though a significant residual activity was conserved.

This decrease could only in part be compensated by an increase (approximately 30%) of SLC25A1 protein abundance as indicated by Western Blotting analysis carried out on cultured skin fibroblasts of the affected brother and control cells (Fig. 3). No evidence of altered mitochondrial content or network morphology was observed (Supplementary Figure 4A) and a small (not significant $p > 0.05$) decrease of mitochondrial membrane potential was measured in patient fibroblasts compared to control cells (Supplementary Figure 4B).

We have recently developed an *in silico* approach to measure the evolutionary constraint acting on each amino acid residue of the human mitochondrial carriers and, consequently, to predict its importance in

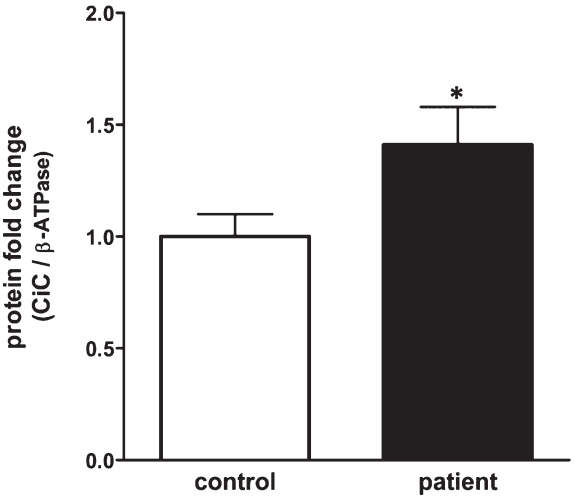

Fig. 3. Total lysates of fibroblast cells (patient and control) were subjected to Western blot analysis upon separation by SDS-PAGE and SLC25A1 (∼31-kDa) and β-ATPase (∼55-kDa) levels were determined by densitometric analysis. The relative ratio was calculated and the means and SDs from three independent experiments are shown (*$p < 0.01$, two-tailed unpaired Student's *t*-test).

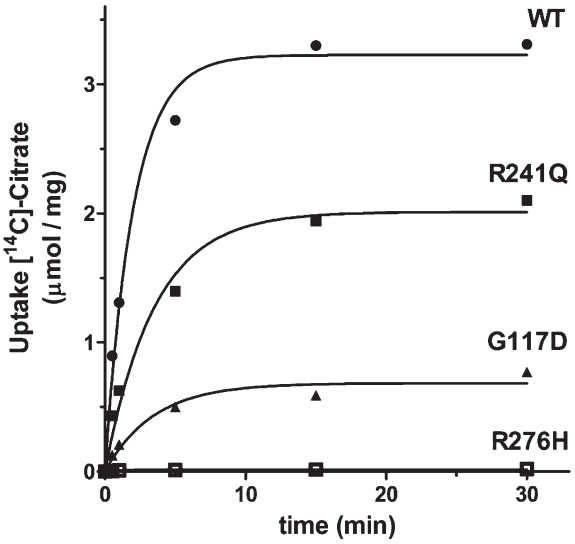

Fig. 4. Transport assay of reconstituted CTP1p wild type (WT) and mutated Ctp1p forms into liposomes. At time zero 0.1 mM (^{14}C) citrate was added to liposomes reconstituted with the recombinant wild-type or mutants and containing 10 mM citrate. At the indicated times, the uptake of the labeled substrate was terminated by adding 20 mM pyridoxal 5′-phosphate and 20 mM bathophenanthroline. Similar results were obtained in four independent experiments.

preserving the carrier function [25]. Considering all the 216 residues previously scored for SLC25A1 [25], R247 is in the bottom 50% of scores, i.e. below a median threshold of 4.68. It is worth noting that all other known mutated residues in SLC25A1-associated pathology have higher scores, including the previously biochemically characterized p.G130D and p.R282H (Table 2, Fig. 4). According to this scoring method, the R247 residue of SLC25A1 is predicted to be less functionally relevant than other mutated SLC25A1 residues, consistent with a milder clinical phenotype, normal levels of urinary 2-hydroxyglutarate and higher protein activity (Table 2).

Zebrafish SLC25A1 knockdown

To explore the effect of reduced expression of SLC25A1 on the neuromuscular junction, we knocked down the 2 SLC25A1 orthologues (SLC25A1a and SLC25A1b) that are expressed in zebrafish embryos, by injection of antisense MOs. Mis-spliced transcripts were detected alongside the wild-type transcript at 48hpf following injection of both SLC25A1a and SLC25A1b MOs (Supplementary Figure 5).

Knockdown of neuromuscular junction proteins usually affects motility and swimming behaviour of injected embryos. Indeed, MO-injected embryos displayed altered tail morphology (Fig. 5), and swimming and touch-evoked escape responses at 48 hpf were impaired. Histologically, we observed normal muscle morphology while NMJ development was abnormal (Figs. 6, 7). Motor axon terminal showed short and erratic outgrowth toward the muscle fibre with no evidence of complete synapse formation, pointing towards an underlying presynaptic defect (Fig. 6). NMJ morphology and function were normal in embryos injected with a standard control MO and in non-injected wild type embryos (data not shown). In addition, knockdown embryos often showed oedema of the hindbrain, heart, yolk sac and tail (Fig. 5, Supplementary Figure 6). Abnormal heart development was observed with increased severity of phenotype with reduced blood flow to the tail (Supplementary video). Knockdown embryos displayed these characteristics in both the presence and absence of the apoptotic suppressing anti-p53 MO (Supplementary Figures 7, 8).

DISCUSSION

The diagnosis of congenital myasthenia is based on the presence of early onset fatigable weakness, impaired NMJ transmission, absence of auto antibodies and response to treatment [5, 31]. The two affected siblings in our study had clinical features consistent with CMS in addition to variable intellectual disability, which is uncommon in CMS. The presence of the high

Table 2
Phenotype and mutations of patients affected by SLC25A1-associated pathologies [17, 18]. A prediction of the functional relevance of each residue is also reported (residue-specific score), as calculated in [25]. (a) agenesis of the corpus callosum and optic nerve hypoplasia with marked jitter on SFEMG(b) neonatal epileptic encephalopathy and absence of developmental progress. (c) Percentage of activity of the mutated yeast orthologous protein compared to the yeast wild-type protein [[17] and this study]. (d) Percentage of citrate uptake in human mutated fibroblasts compared to human control fibroblasts [18]. 2-HG: urinary 2- hydroxyglutarate

Patients	Clinical phenotype	2-HG levels	Human mutation	SLC25A1 Activity (%)	Residue-specific score
Present study	mild	Normal	p.R247Q	40 (c)	3.38
[17]	severe (a)	High	p.G130D	25 (c)	5.50
			p.R282H	0 (c)	5.61
[18] patient 1	severe (b)	High	p.S193W	12.9 (d)	5.51
[18] patient 2	–	High	p.R282G	12.3 (d)	5.61
[18] patient 3	severe (b)	High	p.R282C	6.1 (d)	5.61
[18] patient 5	severe (b)	High	p.G167R	19.8 (d)	5.10
[18] patient 6	severe (b)	High	p.P45L	–	5.00
[18] patient 8	severe (b)	High	p.E144Q	–	5.04
[18] patient 10	severe (b)	High	p.M202T	–	5.33
			p.Y297C	–	4.89

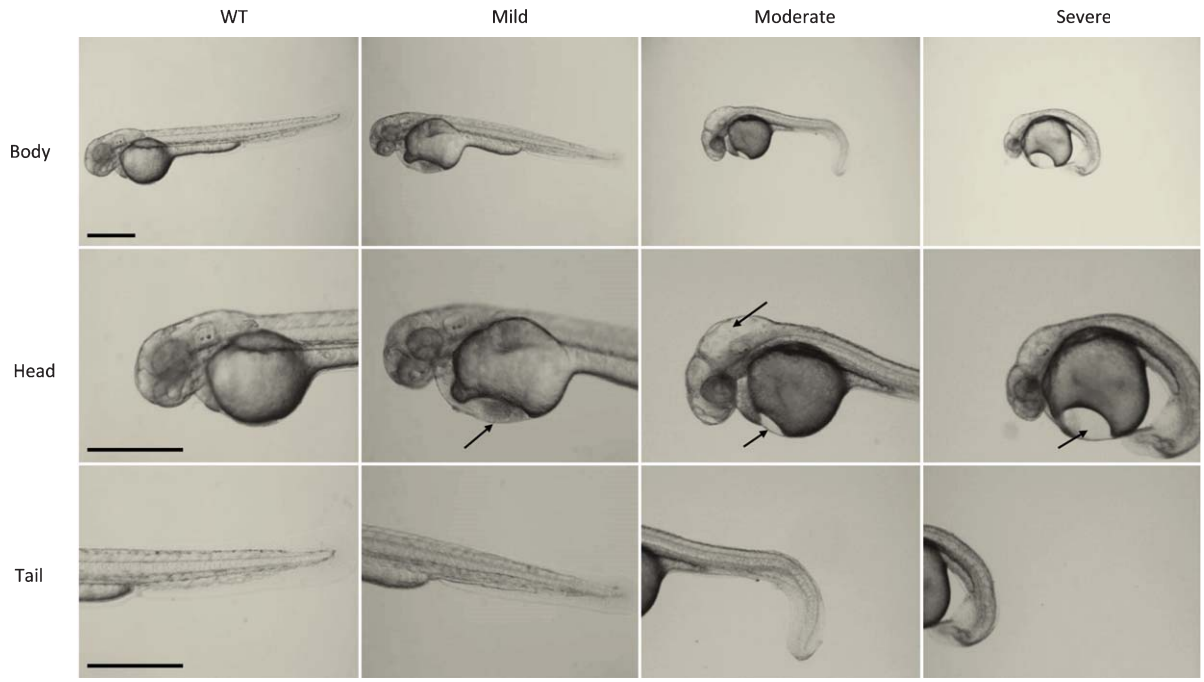

Fig. 5. Live embryos imaged at 48hpf following co-injection of SLC25A1a (5 ng) and SLC25A1b (2.5 ng). Injected embryos demonstrate a range of phenotypes with mild to severe morphological abnormalities. Embryos exhibit a developmental delay with curvature and shortening of the tail and also oedema of the hindbrain, heart, yolk sac and tail. Scale bars: 500 μm.

proportion of pairs showing jitter and the significant blocking on SFEMG, indicated a problem with neuromuscular transmission and thus a contributing NMJ disorder.

It is worth noting that the disease course in these two patients was relatively mild compared to other CMS patients [2], with little evidence of progression.

The X chromosomal deletion identified in the female, but not the male patient could have contributed to her intellectual disability. This is a large heterozygous deletion (30 Mb), which contains 273 genes (full gene list available on request), including *FMR1*, which is responsible for fragile-X-syndrome. In a male individual, a contiguous gene syndrome with a much more severe or probably lethal phenotype would be expected.

We performed homozygosity mapping and whole exome sequencing to determine the underlying genetic cause in our family and successfully identified a novel homozygous mutation in the *SLC25A1* gene. This was

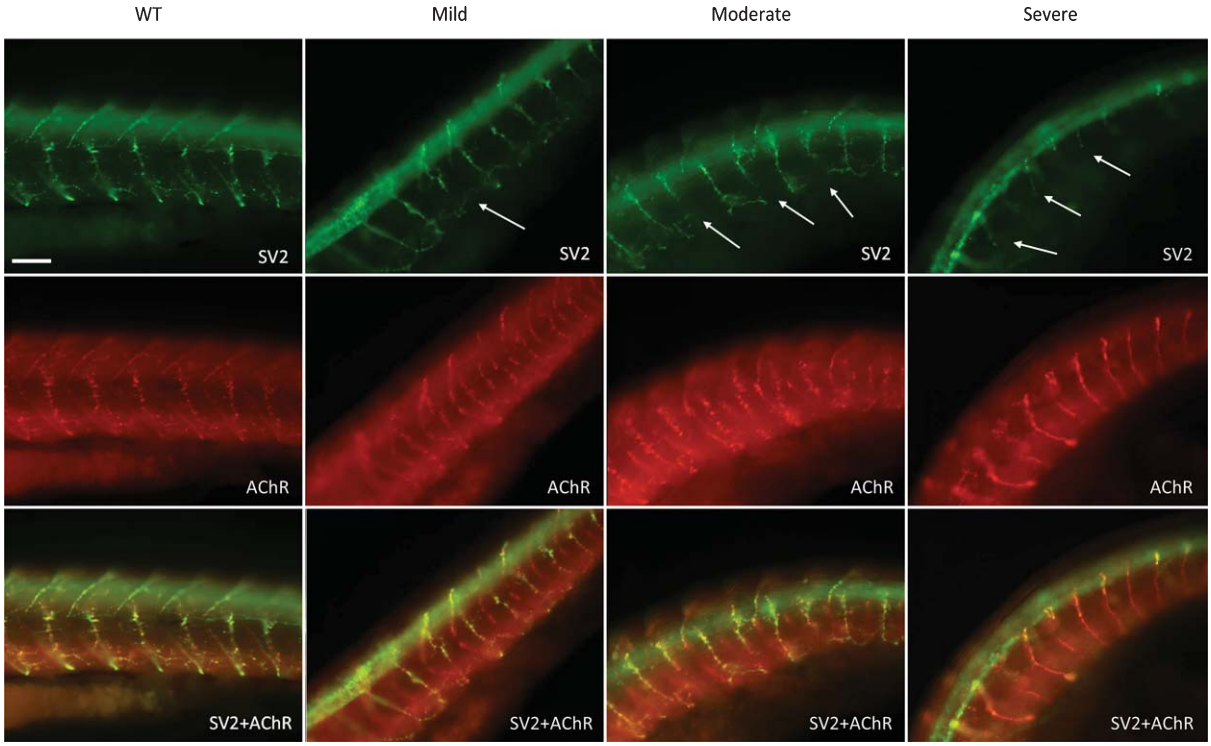

Fig. 6. Neuromuscular junctions following injection with SLC25A1 MOs. Non-injected control Wild Type Golden embryos (left) and SLC25A1 MO injected embryos were stained for postsynaptic AChR (α-bungarotoxin, red staining) and presynaptic nerve endings (SV2 antibody, green staining). Combined SLC25A1 MO (a 5 ng & b 2.5 ng) injected 48hpf embryos demonstrate short motor axons and erratic outgrowth toward the muscle fibre. Scale bar: 50 μm.

the only, novel variant affecting a highly conserved residue, that was expressed in muscle and nerve and predicted to be disease causing. Further corroborating evidence arose from demonstration of a NMJ defect in a previously described patient with a different compound heterozygous mutation of *SLC25A1* gene [17]. The phenotype of the latter was associated with a neurodevelopmental disorder manifesting as profound psychomotor retardation, hypotonia, apnoeic crises, poor feeding, epilepsy, postnatal microcephaly, sensori-neural deafness, agenesis of the corpus callosum (ACC) and hypoplastic optic nerves. She had raised urinary hydroxyglutaric acid levels and Krebs metabolites [17].

In addition, a subsequent report described a series of 13 patients, from 12 unrelated families, with a severe clinical phenotype and recessive *SLC25A1* mutations [18]. 8 of these patients were deceased a few months after birth (range 1 month - 5 years 1 month). All exhibited developmental delay, hypotonia and seizures [18].

A large peak of 2 hydroxyglutaric acid was identified in all patients previously reported with *SLC25A1* mutations, but no variants were identified in corresponding genes causing L2 or D2 hydroxyglutaric aciduria, suggesting that this metabolic disturbance is secondary to defects in *SLC25A1*. We have tested our 2 patients and found normal urinary organic acid analysis in keeping with a milder phenotype. SLC25A1 is well conserved across species and was shown to be critical in intermediary metabolism, glucose induced insulin secretion and chromatin integrity [13, 14, 28, 32]. The chromosomal location of this gene (22q11.2) also attracted some attention as this is either translocated or amplified in some tumours and deleted in DiGeorge syndrome and possibly schizophrenia [33, 34]. However, until recently, *SLC25A1* was not directly linked to any human disease [17, 18].

Knockdown of several CMS genes in zebrafish embryos has been recently used to demonstrate direct or indirect effects on the neuromuscular junction [35, 36]. Interestingly, SLC25A1 knockdown showed variable phenotype ranging from mild, moderate to severe; with confirmed aberrant NMJ development and function similar to what was seen in the 2 affected siblings.

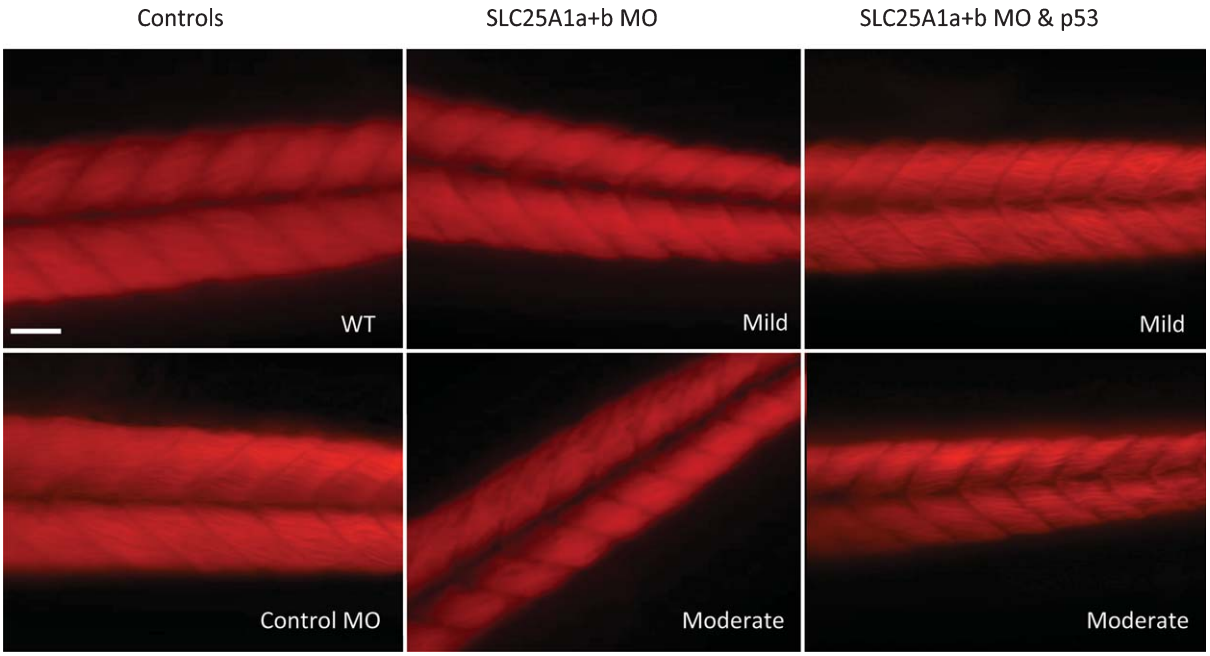

Fig. 7. Muscle morphology following injection with SLC25A1 MOs. WT and control MO injected embryos (left) and SLC25A1 MO injected embryos (centre and right) were stained for F-actin with Alexa Fluor® 594 conjugated phalloidin (5 μg/ml). WT embryos and those injected with a standard control MO showed normal muscle morphology. Combined SLC25A1 MO with and without the addition of anti-p53 MO also demonstrate normal muscle morphology. Scale bar: 50 μm.

At the level of the neuromuscular junction, we were able to show intact muscle fibre architecture with clearly abnormal nerve outgrowth and synapse formation. This indicates that SLC25A1 is required for normal NMJ formation. Of note, an SLC25A1 knockdown zebrafish model was previously generated to show the influence of SLC25A1 on embryogenesis, mitochondrial DNA and autophagy; but limited details of the fish phenotype and NMJ development were provided [14]. In addition to the NMJ abnormalities, we demonstrate further alteration in brain and heart morphology and development in the more severely affected zebrafish morphants, compatible with a more general function of SLC25A1 in mitochondria.

The mutation identified in this study (p.R247Q) has a less deleterious effect when compared to other *SLC25A1* mutations described to date [17, 18]. This is supported by the observed preserved protein expression in patient's skin fibroblast with moderately reduced carrier function and the low score from in *silico* prediction.

In spite of a relevant difference between the scores of R247 and other previously reported mutated residues like G130 [17], the activity of the yeast orthologous protein harboring either of the two pathogenic mutations at equivalent positions is only 15% different, i.e. 40% and 25%, respectively (Table 2 and Fig. 3). Such observation may be the consequence of two possible factors. First, the yeast model system may not exactly reproduce the real activity of the human mutated proteins. Although this cannot be excluded, it appears unlikely since the yeast ortholog closely mirrors SLC25A1 for both protein sequence and citrate transport activity. Furthermore, as far as the clinical phenotype is concerned, it is worth recalling that the p.G130D mutation is heterozygous and the other affected allele harbors the p.R282H mutation [17] which completely abolishes transport activity (Fig. 4). Second, the score is an evolutionary based value, which relies on the strength of natural selection and depends on the fitness of organisms, i.e. the likelihood of organisms to survive and generate fertile progeny [37]. The present patients reached the reproductive age and they may be considered fertile even if the protein activity of the p.R247Q mutant is partially reduced. For this reason the score of p.R247Q is expected to be much lower compared to any other examined *SLC25A1* mutation that is instead responsible for premature death in neonatal age. At the same time, this might explain why G130 and R282 [17] as well other previously reported pathogenic mutations [18] have very close scores.

We speculate that this mild manifestation of disease may have facilitated the detection of an NMJ defect in our patient, while it remains undetected in patients with the more disabling, often fatal form of the disease. Further studies are required to elucidate why the NMJ seems to be particularly sensitive to mild SLC25A1 dysfunction, while other organs such as the brain remain largely asymptomatic. Interestingly, the knockdown experiments in zebrafish show a similar dependency of symptoms in relation to the knockdown: less severely affected zebrafish morphants show motility defects and NMJ abnormalities, but more severely affected morphants have additional defects of the brain and heart compatible with a generalized mitochondrial defect.

Mitochondria are ubiquitous organelles that intervene in a multitude of cellular functions including energy production, cellular metabolism, calcium homeostasis and apoptosis [10, 11]. The exact role of mitochondria in synapse development remains poorly understood and is likely to be complex. How defects in a ubiquitous mitochondrial citrate carrier can manifest primarily as a NMJ defect remains to be determined.

It is also worth emphasizing that *SLC25A1* is likely to be a very rare cause of a pure CMS phenotype. We have screened undiagnosed CMS patients from our extended cohorts and did not detect additional pathogenic *SLC25A1* variants. Exome sequencing results from more than six thousand random individuals (Exome Variant Server; http://evs.gs.washington.edu/EVS/, accessed April 2014), revealed only 15 missense mutations in *SLC25A1*. Each mutation is heterozygous and present in less than 0.1% of the screened population. At least seven of these mutations are predicted to severely impair the protein function according to our scoring system and represent an existing source of pathogenic alleles circulating in the human population. Therefore, while the presence of homozygous mutations or compound heterozygous mutations in *SLC25A1* is a rare event, should a patient show fatigable weakness, one may wish to test for *SLC25A1* mutations and consider screening for cardiac and metabolic defects should this be proven to be culprit.

ACKNOWLEDGMENTS

The authors would like to thank all the patients for taking part in this study. The Institute of Genetic Medicine in Newcastle is part of the MRC Centre for Neuromuscular Diseases and the TREAT-NMD Alliance (www.treat-nmd.eu). This study was supported by the Medical Research Council UK (reference G1002274, grant ID 98482), by the European Union Seventh Framework Programme (FP7/2007-2013) under grant agreement No. 305444 (RD-Connect) and 305121 (Neuromics), by the Myasthenia Gravis Association and by grants from the University of Bari (Fondi di Ateneo) and by the Center of Excellence in Comparative Genomics (CEGBA).

The SV2 monoclonal antibody developed by Kathleen Buckley was obtained from the Developmental Studies Hybridoma Bank developed under the auspices of the NICHD and maintained at The University of Iowa, Department of Biology, Iowa City, IA 52242.

SUPPLEMENTARY MATERIAL

Supplementary material is available in the electronic version of this article: http://dx.doi.org/10.3233/JND-140021.

Supplementary Video. Video footage of 48hpf zebrafish embryos following co-injection of SLC25A1a (5 ng) and SLC25A1b (2.5 ng): Mildly (Top Right), moderately (Bottom Left), and severely (Bottom Right) affected embryos demonstrate a reduced heart rate compared to that of the non-injected Wild Type Golden control embryos (Top Left)".

Supplementary Figure 1. RT-PCR analysis of SLC25A1 orthologs at different stages of zebrafish development. Both SLC25A1 genes on Chr.10 (SLC25A1a & SLC25A1b) are expressed from 0.5 hours post fertilisation (hpf) and maintained throughout development into adulthood. SLC25A1 gene on Chr.8 is not expressed during zebrafish development or adulthood. EF1α: elongation factor 1 alpha was used as internal RT-PCR control for all time points to certify cDNA synthesis quality.

Supplementary Figure 2. Structural comparative model of human CIC and docking of citrate. The 3D comparative model of human CIC is reported in white cartoon representation. The six transmembrane helices are indicated by black labels (H1-H6). The three short helices parallel to the membrane planes are also labelled (h12, h34, and h56). The citrate ligand is shown in cyan licorice. The residues forming the m-gate are reported in black mesh representation. Panel (A): lateral view of the human citrate carrier. Prolines (magenta beads) and glycines (yellow beads) of the PG levels (or the corresponding residues) surround the substrate binding area. The pathogenic mutations R247Q (this work), G130D and R282H are reported

in red surf representation and are indicated by black labels. Panel (B): Bottom view of the 3D comparative model of human CIC. The pathogenic mutation R247Q is reported in magenta licorice representation. R247 and E270 are reported in yellow sticks representation. Black dashed lines indicate ionic bonds (both shorter than 2.5 Å). The symmetrical interactions observed on the first and on the second repeat (K174-E149 and Q52-H78, shown in white sticks representation) are also reported for comparative purposes. Red dashed lines indicate putative (water mediated) H-bond interactions (among 5.5 and 6.5 Å).

Supplementary Figure 3. Exploded view of the salt bridge between R247 and E270 (panel A) and of the putative H-bond interactions between Q247 and E270 (panel B). Colours and graphical representations as in Supplementary Figure 2.

Supplementary Figure 4. Mitochondrial staining in fibroblast cells relative to control and patient (panel A). Mitochondrial Staining with Mitotracker Mitochondrion-selective Probes- Medium containing Mitotracker Red CMXRos in a range of 10–500 nM was added to cells grown on tissue culture chamber slides and incubated at 37°C for 30–45 min. After incubation, the medium containing the Mitotracker dye was replaced with fresh medium, and the stained cells were observed by fluorescence microscopy. The same cells were used to measure mitochondrial membrane potential using the tetramethylrhodamine methyl ester (TMRM) probe. $\Delta\Psi$ measured as relative fluorescence units (RFU) is presented as mean $\pm$ SD of three experiments (panel B).

Supplementary Figure 5. RT-PCR analysis of SLC25A1a and SLC25A1b MO induced phenotypes at different stages of zebrafish development. Both SLC25A1a & SLC25A1b induce splicing of the associated genes on Chr.10 at both 24hpf and 48hpf.

Supplementary Figure 6. Percentage of phenotypes observed in zebrafish following injection of SLC25A1a+b MO in the presence and absence of anti-p53 MO compared to non-injected control and control MO injected embryos. Non-injected control embryos and those injected with a standard control MO showed similar percentage of survival. Combined SLC25A1 MO with and without the addition of anti-p53 MO demonstrate reduced percentage of survival. Co-injection with anti-p53 MO displays a reduced percentage of severe phenotypes observed.

Supplementary Figure 7. Morphology of 48hpf SLC25A1 morphant embryos. Live embryos imaged at 48hpf following co-injection of SLC25A1a (5 ng), SLC25A1b (2.5 ng) and anti-p53 MO. Embryos were injected with an anti-p53 MO, suppressing the non-specific MO mediated apoptotic affects produced by p53 activation. Injected embryos also demonstrated a range of phenotypes from mildly to severely affected. Embryos exhibit a developmental delay with curvature and shortening of the tail and also oedema of the hindbrain, heart, yolk sac and tail. Scale bars: 500 μm.

Supplementary Figure 8. Neuromuscular junctions following injection with SLC25A1 MOs and anti-p53 MO. Embryos injected with a standard control MO showed no signs of neuronal abnormality and were indistinguishable from non-injected wild type embryos. WilSLC25A1 MO injected embryos (centre and right) were stained for postsynaptic AChR (α-bungarotoxin, red staining) and presynaptic nerve endings (SV2 antibody, green staining). Combined SLC25A1 MO (a 5 ng & b 2.5 ng) with the addition of anti-p53 MO injected 48hpf embryos also exhibit shortening and branching of motor axons. Scale bar: 50 μm.

CONFLICT OF INTEREST

The authors have no conflict of interest to declare.

REFERENCES

[1] Beeson, D. Synaptic dysfunction in congenital myasthenic syndromes. Annals of the New York Academy of Sciences. 2012; 1275: 63-69.

[2] Chaouch, A., Beeson, D., Hantai, D., and Lochmuller, H. 186th ENMC international workshop: Congenital myasthenic syndromes 24-26 June 2011, Naarden, The Netherlands. Neuromuscular Disorders: NMD. 2012; 22(6): 566-576.

[3] Barisic, N., Chaouch, A., Muller, J. S., and Lochmuller, H. Genetic heterogeneity and pathophysiological mechanisms in congenital myasthenic syndromes. Eur J Paediatr Neurol. 2011; 15(3): 189-196.

[4] Engel, A. G. Current status of the congenital myasthenic syndromes. Neuromuscular Disorders: NMD. 2012; 22(2): 99-111.

[5] Hantai, D., Nicole, S., and Eymard, B. Congenital myasthenic syndromes: An update. Current Opinion in Neurology. 2013; 26(5): 561-568.

[6] Belaya, K., Finlayson, S., Slater, C. R., Cossins, J., Liu, W. W., Maxwell, S., et al. Mutations in DPAGT1 cause a limb-girdle congenital myasthenic syndrome with tubular aggregates. American Journal of Human Genetics. 2012; 91(1): 193-201.

[7] Cossins, J., Belaya, K., Hicks, D., Salih, M. A., Finlayson, S., Carboni, N., et al. Congenital myasthenic syndromes due to mutations in ALG2 and ALG14. Brain: A Journal of Neurology. 2013; 136(Pt 3): 944-956.

[8] Forrest, K., Mellerio, J. E., Robb, S., Dopping-Hepenstal, P. J., McGrath, J. A., Liu, L., et al. Congenital muscular dystrophy, myasthenic symptoms and epidermolysis bullosa simplex (EBS) associated with mutations in the PLEC1 gene encoding plectin. Neuromuscular Disorders: NMD. 2010; 20(11): 709-711.

[9] Maselli, R. A., Ng, J. J., Anderson, J. A., Cagney, O., Arredondo, J., Williams, C., et al. Mutations in LAMB2 causing a severe form of synaptic congenital myasthenic syndrome. Journal of Medical Genetics. 2009; 46(3): 203-208.

[10] McFarland, R., Taylor, R. W., and Turnbull, D. M. A neurological perspective on mitochondrial disease. Lancet neurology. 2010; 9(8): 829-840.

[11] Ly, C. V., and Verstreken, P. Mitochondria at the synapse. The Neuroscientist: A Review Journal Bringing Neurobiology, Neurology and Psychiatry. 2006; 12(4): 291-299.

[12] Kaplan, R. S., Mayor, J. A., and Wood, D. O. The mitochondrial tricarboxylate transport protein. cDNA cloning, primary structure, and comparison with other mitochondrial transport proteins. The Journal of Biological Chemistry. 1993; 268(18): 13682-13690.

[13] Morciano, P., Carrisi, C., Capobianco, L., Mannini, L., Burgio, G., Cestra, G., et al. A conserved role for the mitochondrial citrate transporter Sea/SLC25A1 in the maintenance of chromosome integrity. Human Molecular Genetics. 2009; 18(21): 4180-4188.

[14] Catalina-Rodriguez, O., Kolukula, V. K., Tomita, Y., Preet, A., Palmieri, F., Wellstein, A., et al. The mitochondrial citrate transporter, CIC, is essential for mitochondrial homeostasis. Oncotarget. 2012; 3(10): 1220-1235.

[15] Moraes, T. F., and Reithmeier, R. A. Membrane transport metabolons. Biochimica et Biophysica Acta. 2012; 1818(11): 2687-2706.

[16] Sun, J., Aluvila, S., Kotaria, R., Mayor, J. A., Walters, D. E., and Kaplan, R. S. Mitochondrial and plasma membrane citrate transporters: Discovery of selective inhibitors and application to structure/function analysis. Molecular and Cellular Pharmacology. 2010; 2(3): 101-110.

[17] Edvardson, S., Porcelli, V., Jalas, C., Soiferman, D., Kellner, Y., Shaag, A., et al. Agenesis of corpus callosum and optic nerve hypoplasia due to mutations in SLC25A1 encoding the mitochondrial citrate transporter. Journal of Medical Genetics. 2013; 50(4): 240-245.

[18] Nota, B., Struys, E. A., Pop, A., Jansen, E. E., Fernandez Ojeda, M. R., Kanhai, W. A., et al. Deficiency in SLC25A1, encoding the mitochondrial citrate carrier, causes combined D-2- and L-2-hydroxyglutaric aciduria. American Journal of Human Genetics. 2013; 92(4): 627-631.

[19] Vincent, A., Cullcandy, S. G., Newsomdavis, J., Trautmann, A., Molenaar, P. C., and Polak, R. L. Congenital myasthenia - endplate acetylcholine-receptors and electrophysiology in 5 cases. Muscle & Nerve. 1981; 4(4): 306-318.

[20] Fiermonte, G., Walker, J. E., and Palmieri, F. Abundant bacterial expression and reconstitution of an intrinsic membrane-transport protein from bovine mitochondria. The Biochemical Journal. 1993; 294(Pt 1): 293-299.

[21] Palmieri, F., Indiveri, C., Bisaccia, F., and Iacobazzi, V. Mitochondrial metabolite carrier proteins: Purification, reconstitution, and transport studies. Methods in Enzymology. 1995; 260: 349-369.

[22] Scaduto, R. C., Jr., and Grotyohann, L. W. Measurement of mitochondrial membrane potential using fluorescent rhodamine derivatives. Biophysical Journal. 1999; 76(1 Pt 1): 469-477.

[23] Lasorsa, F. M., Scarcia, P., Erdmann, R., Palmieri, F., Rottensteiner, H., and Palmieri, L. The yeast peroxisomal adenine nucleotide transporter: Characterization of two transport modes and involvement in DeltapH formation across peroxisomal membranes. The Biochemical Journal. 2004; 381(Pt 3): 581-585.

[24] Persson, B. Bioinformatics in protein analysis. Exs. 2000; 88: 215-231.

[25] Pierri, C. L., Palmieri, F., and De Grassi, A. Single-nucleotide evolution quantifies the importance of each site along the structure of mitochondrial carriers. Cellular and molecular life sciences: CMLS. 2014; 71(2): 349-364.

[26] Palmieri, F., Agrimi, G., Blanco, E., Castegna, A., Di Noia, M. A., Iacobazzi, V., et al. Identification of mitochondrial carriers in Saccharomyces cerevisiae by transport assay of reconstituted recombinant proteins. Bba-Bioenergetics. 2006; 1757(9-10): 1249-1262.

[27] Fontanesi, F., Palmieri, L., Scarcia, P., Lodi, T., Donnini, C., Limongelli, A., et al. Mutations in AAC2, equivalent to human adPEO-associated ANT1 mutations, lead to defective oxidative phosphorylation in Saccharomyces cerevisiae and affect mitochondrial DNA stability. Human Molecular Genetics. 2004; 13(9): 923-934.

[28] Palmieri, F. The mitochondrial transporter family SLC25: Identification, properties and physiopathology. Molecular Aspects of Medicine. 2013; 34(2-3): 465-484.

[29] Pebay-Peyroula, E., Dahout-Gonzalez, C., Kahn, R., Trezeguet, V., Lauquin, G. J., and Brandolin, G. Structure of mitochondrial ADP/ATP carrier in complex with carboxyatractyloside. Nature. 2003; 426(6962): 39-44.

[30] Palmieri, F., and Pierri, C. L. Structure and function of mitochondrial carriers - role of the transmembrane helix P and G residues in the gating and transport mechanism. FEBS Letters. 2010; 584(9): 1931-1939.

[31] Beeson, D., Hantai, D., Lochmuller, H., and Engel, A. G. 126th International Workshop: Congenital myasthenic syndromes, 24-26 September 2004, Naarden, the Netherlands. Neuromuscular disorders: NMD. 2005; 15(7): 498-512.

[32] Iacobazzi, V., Infantino, V., Bisaccia, F., Castegna, A., and Palmieri, F. Role of FOXA in mitochondrial citrate carrier gene expression and insulin secretion. Biochemical and Biophysical Research Communications. 2009; 385(2): 220-224.

[33] Maynard, T. M., Meechan, D. W., Dudevoir, M. L., Gopalakrishna, D., Peters, A. Z., Heindel, C. C., et al. Mitochondrial localization and function of a subset of 22q11 deletion syndrome candidate genes. Molecular and Cellular Neurosciences. 2008; 39(3): 439-451.

[34] Williams, N. M., Spurlock, G., Norton, N., Williams, H. J., Hamshere, M. L., Krawczak, M., et al. Mutation screening and LD mapping in the VCFS deleted region of chromosome 22q11 in schizophrenia using a novel DNA pooling approach. Molecular Psychiatry. 2002; 7(10): 1092-1100.

[35] Muller, J. S., Jepson, C. D., Laval, S. H., Bushby, K., Straub, V., and Lochmuller, H. Dok-7 promotes slow muscle integrity as well as neuromuscular junction formation in a zebrafish model of congenital myasthenic syndromes. Human Molecular Genetics. 2010; 19(9): 1726-1740.

[36] Senderek, J., Muller, J. S., Dusl, M., Strom, T. M., Guergueltcheva, V., Diepolder, I., et al. Hexosamine biosynthetic pathway mutations cause neuromuscular transmission defect. American Journal of Human Genetics. 2011; 88(2): 162-172.

[37] Eyre-Walker, A., and Keightley, P. D. The distribution of fitness effects of new mutations. Nature Reviews Genetics. 2007; 8(8): 610-618.

[38] Li, H., and Durbin, R. Fast and accurate short read alignment with Burrows-Wheeler transform. Bioinformatics. 2009; 25(14): 1754-1760.

[39] Albers, C. A., Lunter, G., MacArthur, D. G., McVean, G., Ouwehand, W. H., and Durbin, R. Dindel: Accurate indel

calls from short-read data. Genome Research. 2011; 21(6): 961-973.

[40] Wang, K., Li, M., and Hakonarson, H. ANNOVAR: Functional annotation of genetic variants from high-throughput sequencing data. Nucleic Acids Res. 2010; 38(16): e164.

[41] Kent, W. J., Sugnet, C. W., Furey, T. S., Roskin, K. M., Pringle, T. H., Zahler, A. M., et al. The human genome browser at UCSC. Genome Research. 2002; 12(6): 996-1006.

[42] Sanchez, R., and Sali, A. Comparative protein structure modeling. Introduction and practical examples with modeller. Methods in Molecular Biology. 2000; 143: 97-129.

[43] Pebay-Peyroula, E., Dahout-Gonzalez, C., Kahn, R., Trezeguet, V., Lauquin, G. J. M., and Brandolin, R. Structure of mitochondrial ADP/ATP carrier in complex with carboxyatractyloside. Nature. 2003; 426(6962): 39-44.

[44] Morris, G. M., Huey, R., and Olson, A. J. Using AutoDock for ligand-receptor docking. Current protocols in bioinformatics/editoral board, Andreas D Baxevanis [et al.], 2008; Chapter 8: Unit 8 14.

[45] Palmieri, F., and Pierri, C. L. Mitochondrial metabolite transport. Essays in Biochemistry. 2010; 47: 37-52.

[46] Robinson, A. J., Overy, C., and Kunji, E. R. The mechanism of transport by mitochondrial carriers based on analysis of symmetry. Proceedings of the National Academy of Sciences of the United States of America. 2008; 105(46): 17766-17771.

[47] Klingenberg, M. Ligand-protein interaction in biomembrane carriers. The induced transition fit of transport catalysis. Biochemistry. 2005; 44(24): 8563-8570.

[48] Kunji, E. R., and Robinson, A. J. The conserved substrate binding site of mitochondrial carriers. Biochimica et Biophysica Acta. 2006; 1757(9-10): 1237-1248.

[49] Falconi, M., Chillemi, G., Di Marino, D., D'Annessa, I., Morozzo della Rocca, B., Palmieri, L., et al. Structural dynamics of the mitochondrial ADP/ATP carrier revealed by molecular dynamics simulation studies. Proteins. 2006; 65(3): 681-691.